



Selective hydrogenation of citral by noble metals supported on carbon xerogels: Catalytic performance and stability

Esther Bailón-García, Francisco Carrasco-Marín, Agustín F. Pérez-Cadenas,
Francisco J. Maldonado-Hódar*

Research Group in Carbon Materials, Inorganic Chemistry Department, Faculty of Sciences, University of Granada, Campus Fuentenueva s/n., 18071 Granada, Spain

ARTICLE INFO

Article history:

Received 29 October 2015

Received in revised form 9 December 2015

Accepted 16 December 2015

Available online 21 December 2015

Keywords:

Selective hydrogenation

Citral

Active phase selection

Catalyst deactivation

ABSTRACT

A series of monometallic Pt, Ir and Ru-catalysts deposited on carbon xerogel microspheres was prepared, exhaustively characterized and used in the selective hydrogenation of citral. A similar metal particle size is obtained in all cases after He-pretreatment, allowing the comparison between metals; the catalytic activity increases in the sense Ir < Ru < Pt. Sintering is favoured when catalysts are pretreated in H₂-flow leading to an important loss of activity, especially for Ru-catalysts. Pt and Ir-catalysts are more selective than Ru-catalysts, reaching selectivity values to unsaturated alcohols of around 80%. Thus, in terms of yields to these valuable products Pt-catalysts seem to be the most appropriate active phase. Nevertheless, reutilization experiments showed that Ir-catalyst maintained a good performance while a severe deactivation is observed for Pt-catalysts. This fact is discussed on the basis of the different nature of the deposits formed during reaction.

© 2015 Elsevier B.V. All rights reserved.

1. Introduction

The selective hydrogenation of carbonyl groups of α,β-unsaturated aldehydes, to produce unsaturated alcohols (UA), is a challenging process either from a scientific or economic point of view [1–3]. The selective hydrogenation of citral is one of the more feasible ways to obtain nerol and geraniol, molecules with a high demand for the pharmaceutical or chemical industry. Furthermore, citral has very recently come to be produced petrochemically in very large quantities, and partial hydrogenation of citral has become a very interesting economical route due to it would be a single step synthesis in contrast with the actual long and complicated synthesis procedure [4]. Therefore, the hydrogenation of citral is attracting the attention of a large number of scientists worldwide.

Nevertheless, the selective hydrogenation of citral to UA (nerol and geraniol) is not easy, because citral possesses three potentially hydrogenable double bonds: an isolated C=C bond in addition to conjugated C=O and C=C bonds. Thermodynamic and kinetic reasons favor the hydrogenation of the C=C over the C=O group and thus even in the presence of most of conventional hydrogenation catalysts, the saturated aldehyde or alcohol (instead of the unsat-

urated ones) are obtained as main reaction products [5,6]. Fig. 1 shows the reaction scheme of the citral hydrogenation

In the catalyst design for the hydrogenation of α,β-unsaturated aldehydes there are several important issues which affect the catalysts performance and product distribution including the nature of the active metal and supports used [7–9], the catalyst preparation method (catalyst precursor, pretreatments, etc) [10,11], dispersion of the active phase and interaction with the support, the addition of a second metal [10–13], as well as other factors relating to the operating conditions as solvent (which is important in the formation of acetals), stirring, temperature, H₂-pressure and initial reactant/catalyst concentration.

Regarding the catalytic phase, not only the performance, but also economic factors related with the stability, regeneration and price, should be considered. In general, transition metals are used as active phase. Vannice and Singh [6] show that the catalytic activity in citral hydrogenation varies as: Pd > Pt > Ir > Os > Ru > Rh > Ni > Co » Fe. Catalysts based in Os showed a high selectivity to unsaturated alcohols ($S_{UA} = 88\%$), Ru and Co showed a moderate S_{UA} (55%) but, Pt, Ir, Rh, Ni and Pd were more selective to citronellal and isopulegol (0% unsaturated alcohols).

Several studies show also the importance of the support [7,14,15] on the catalyst performance. In previous manuscripts, we conclude that carbon xerogels offer several advantages as Pt-support regarding inorganic oxides [14] and even other carbon

* Corresponding author.

E-mail address: fjmaldon@ugr.es (F.J. Maldonado-Hódar).

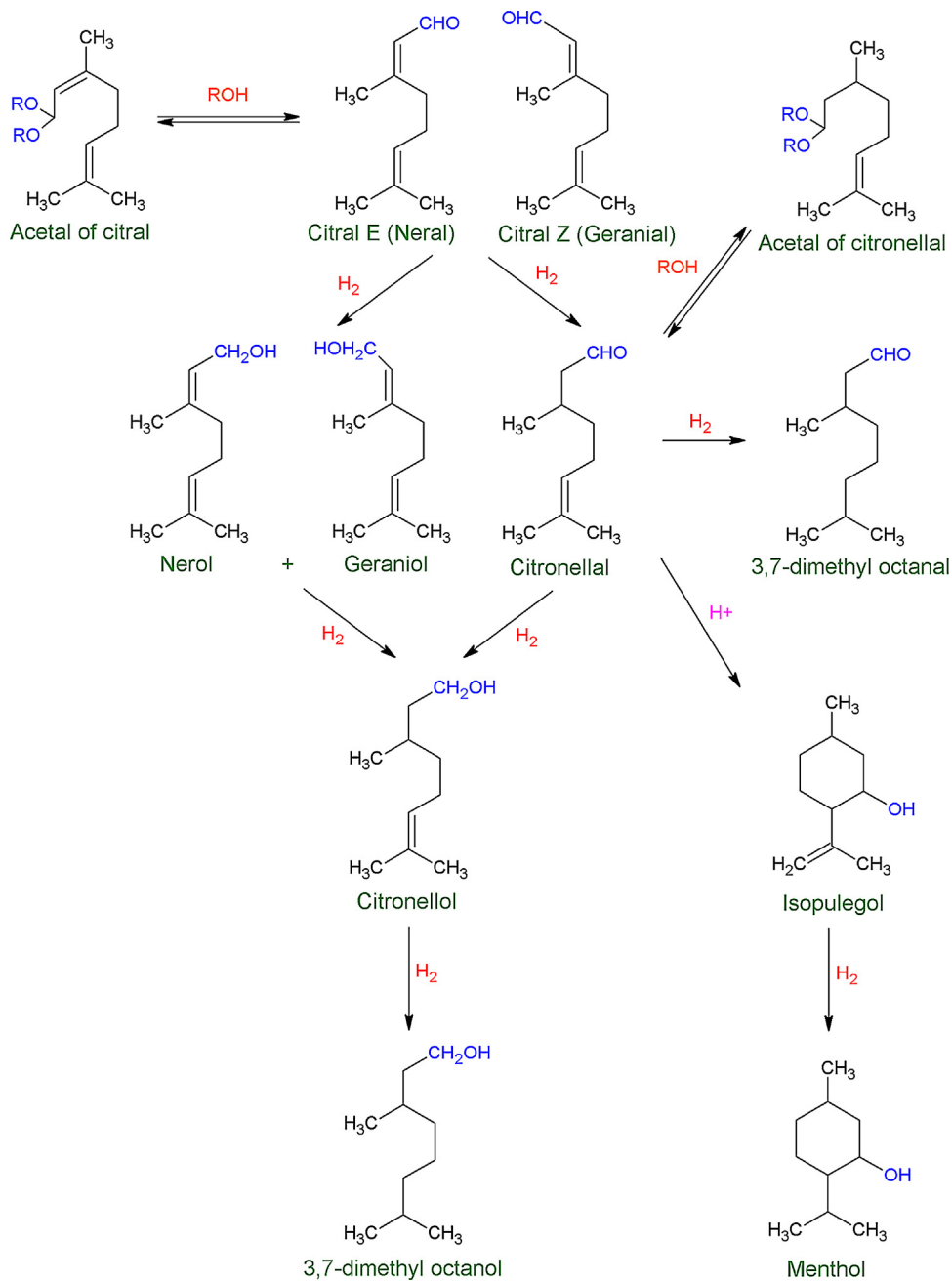


Fig. 1. Reaction scheme of the citral hydrogenation.

materials [15] on the basis of purity, absence of acidity and a defined morphology and porous texture. Moreover, the catalytic performance clearly is based on the combination of the support/active phase characteristics and their interactions. This fact was early studied by Sokol'skii [16] and Giroir-Fendler et al. [17], in the crotonaldehyde and cinnamaldehyde hydrogenation, respectively. They described a high selectivity to crotyl alcohol when Pt and Os are supported on Fe₂O₃. However, using carbon supports, a similar S_{UA} value (around 75%) using Ir, with Pt and Ru is obtained while selectivity is moderate and poor using Rh and Pd. The S_{UA} of Pt and Ru-catalysts dramatically increased when supported on graphite regarding activated carbons, while Ir has a high intrinsic selectivity which is not modified by the carbon nature.

On the contrary, strong variations in the performance of Ir-catalysts were described by different authors [5,7]. Thus, using Ir/TiO₂, S_{UA} reached values as high as 91–100% [18,19] while other

authors get only a moderate selectivity of 60% [20] with similar catalytic systems and operating conditions. Also, using Ir/SiO₂ catalysts very different selectivity values, among 100% [18], 40% [21] or 15% [8], were obtained. Nevertheless, all of these studies agree with the poor activity of Ir-catalysts, where conversion values typically present values smaller than 15% [7].

These variations in the S_{UA} values depending on the nature of supports/active phase were attributed to electronic transfers. The S_{UA} seem to be correlated with the metal d-band width, according to theoretical calculations of Delbecq and Sautet and semi-empirical calculations of Hückel [2,22]. With increasing electron density and hence d-orbital population, the repulsive electron interaction of the metal with the C=C double bond increase and the interaction of the metal surface with the C=O π-system is favoured [5,23]. Thus, in general it is described that independently on the support, Pd, Rh and Ni-catalysts are unselective to unsaturated alcohol, moderate

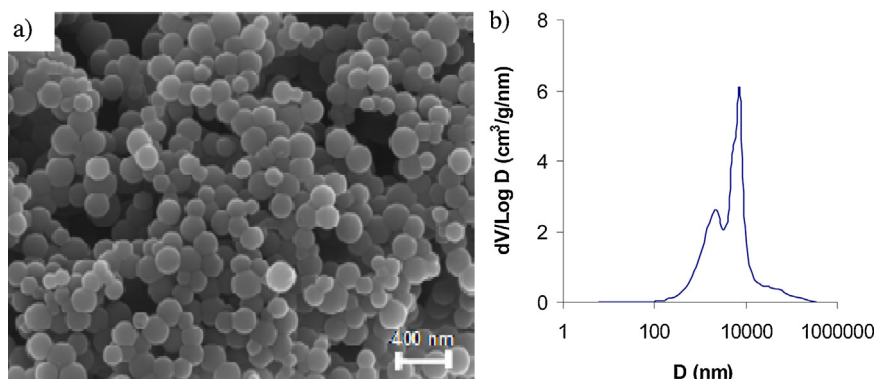


Fig. 2. (a) SEM image showing the morphology of A8-support and (b) the PSD obtained by mercury porosimetry.

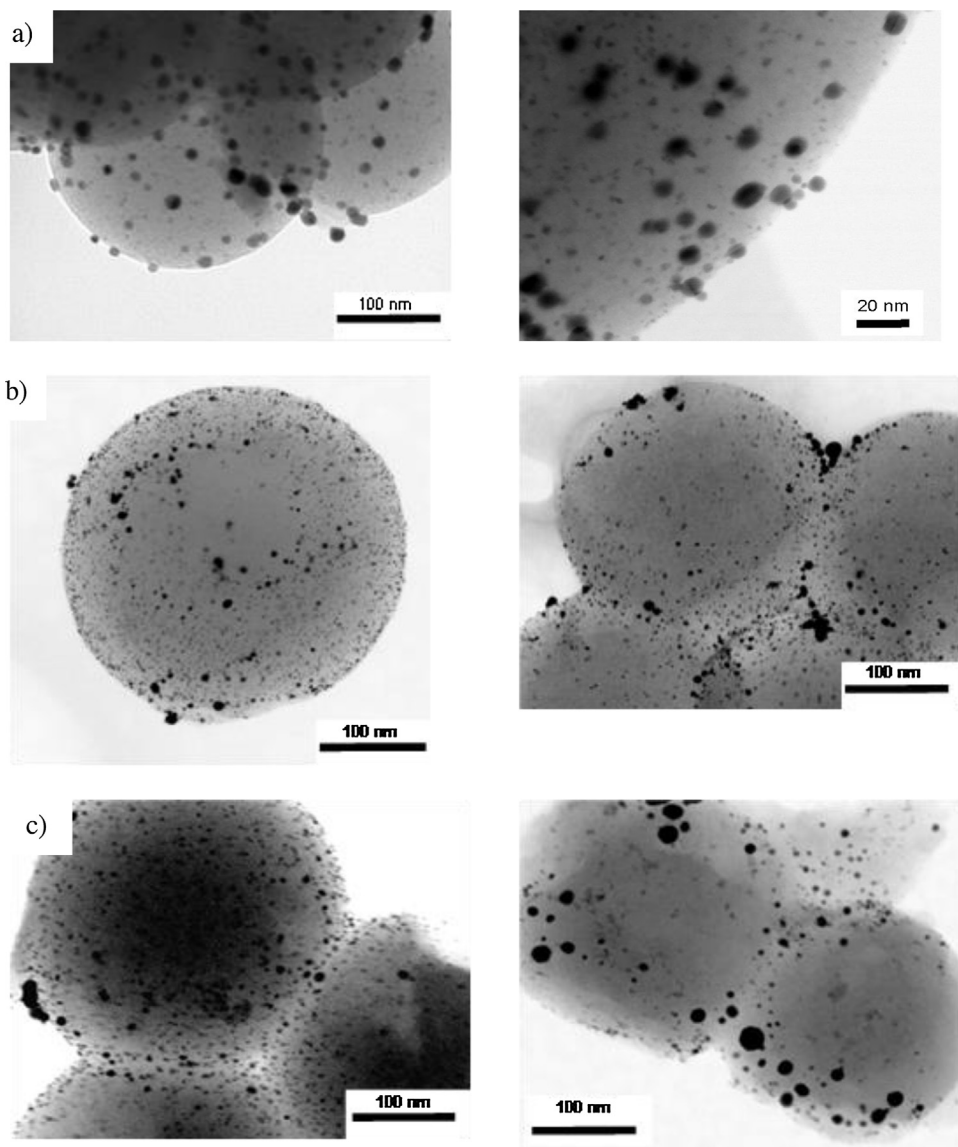


Fig. 3. HRTEM images of catalysts after He (left) or H₂-pretreatment (right). (a) Pt, (b) Ir and (c) Ru-catalysts.

selectivity values are achieved using Ru-catalysts while those based on Os are highly selective. As commented, there is however a great dispersion of results regarding the behavior of Pt and Ir-catalysts.

In previous manuscripts [14,15] we studied the role of different inorganic and carbon supports looking for the development

of selective hydrogenation catalysts and conclude that carbon xerogels structured in independent microspheres present the best combination of chemical and porous properties to enhance the catalytic performance. Once selected the support, in this manuscript, the influence of the active phase is analyzed to find the best

Table 1

Textural characteristics of carbon support and metal-catalysts after the corresponding pretreatment.

Sample	Pretreatment Conditions	N ₂ -adsorption					CO ₂ -adsorption		
		S _{BET} m ² g ⁻¹	W ₀ cm ³ g ⁻¹	L ₀ nm	V _{meso} cm ³ g ⁻¹	V _{0.95} cm ³ g ⁻¹	W ₀ cm ³ g ⁻¹	S _{mic} m ² g ⁻¹	L ₀ nm
A8	–	614	0.25	0.78	0.00	0.31	0.29	952	0.60
A8Pt3-5	He/400 °C	553	0.22	0.64	0.00	0.25	0.28	965	0.58
A8Pt3-8	H ₂ /400 °C	521	0.21	0.60	0.00	0.22	0.28	960	0.58
A8Ir3-	He/400 °C	578	0.23	0.73	0.00	0.32	0.29	933	0.62
A8Ir3-	H ₂ /400 °C	595	0.24	0.50	0.00	0.31	0.30	997	0.61
A8Ru3-	He/400 °C	573	0.23	0.72	0.00	0.31	0.28	913	0.62
A8Ru3-	H ₂ /400 °C	404	0.15	0.91	0.00	0.26	0.24	749	0.63

Table 2

Mean metal-particle size determined by H₂-chemisorption (\bar{d}_{H_2}) and HRTEM (\bar{d}_{TEM}). XPS results: metal-surface concentration (M_{XPS}, %Wt.), binding energy (B.E.) of metal-species detected (M⁰ and M^{II}) and their proportions (%).

Catalyst	\bar{d}_{H_2} (nm)	\bar{d}_{TEM} (nm)	M _{XPS} (%Wt)	M ⁰ BE (eV)	M ⁰ (%)	M ^{II} BE (eV)	M ^{II} (%)
A8Pt3-5	5.1	7.2	7.0	71.3	72	72.5	28
A8Pt3-8	7.9	9.3	4.4	71.3	70	72.3	30
A8Ir3-4	4.4	3.0	6.1	61.2	64	62.2	36
A8Ir3-5	5.2	3.4	5.8	61.3	66	62.2	34
A8Ru3-5	5.0	5.4	7.4	462.5	69	464.8	31
A8Ru3-13	13.4	7.5	5.1	462.2	70	464.2	30

Table 3

Comparison of the initial reaction rate and products distribution.

Sample	r ₀ , mol/l/s × 10 ⁶	S _{UA} (%)	S _{Cal} (%)	S _{Col} (%)	S _{3,7DMO} (%)	S _{Isop + Ment} (%)
A8Pt3-5	2.18	41.9	38.7	10.4	5.7	3.3
A8Pt3-8	1.63	35.6	46.0	10.7	4.2	3.5
A8Ir3-4	0.41	60.0	20.5	14.3	5.2	0.0
A8Ir3-5	0.47	64.7	24.5	6.6	2.8	1.4
A8Ru3-5	0.60	40.8	50.6	8.6	0.0	0.0
A8Ru3-13	0.31	36.7	46.5	11.9	4.9	0.0

Note: Selectivity values at 5% of conversion; UA: unsaturated alcohols, Cal: citronellal, Col: citronellol, 3,7DMO: 3,7 dimethyloctanol, Isop: isopulegol, Ment: menthol.

support/active phase combination. The characteristics of Pt, Ir and Ru catalysts obtained by the same preparation procedure are studied, establishing relationships between these properties and the catalytic performance and stability of samples.

2. Experimental

The carbon xerogel (A8) was prepared by polycondensation of resorcinol with formaldehyde in aqueous media, using Cs₂CO₃ as a polymerization catalyst by modifying a previous synthesis procedure [24]. The synthesis procedure was published elsewhere [14,15]. In brief, the proper amount of resorcinol and Cs₂CO₃ were added to deionised water in a three-necks glass reactor provided of reflux, controlled temperature (85 °C) and stirring. Then, formaldehyde solution (Sigma, 37 wt%) was added dropwise in the flask under agitation (250 rpm) and the gel formed was aged at 85 °C for 24 h. Finally, the suspension was filtered and placed in acetone (3 days, changing acetone twice daily) to exchange water within the pores by acetone, in order to reduce the porosity collapse during the subsequent drying process [25]. The gel was dried by microwave using a Saivod MS-287W microwave oven under nitrogen atmosphere in periods of 1 min at 384 W until constant weight and carbonized to obtain the corresponding carbon xerogel in N₂ flow at 150 cm³/min, heating to 900 °C at a heating rate of 1 °C/min, in order to allow a soft removing of pyrolysis gases, and soaking time of 2 h. The carbon xerogel obtained is called A8.

This support was milled and sieved to a diameter smaller than 0.150 mm before impregnation. Platinum, iridium and ruthenium catalysts were prepared by impregnation at 3 wt% Metal-loading using an aqueous solution that contains the appropriate amount of [Pt(NH₃)₄]Cl₂, IrCl₄ and RuCl₃, respectively and pretreated in He or

H₂ flow at 400 °C (heating rate of 5 °C/min) for 12 h. Catalysts were referred to based on the support, the metal-content and the final mean metal-particle size determined by H₂-chemisorption. Thus, as an example, A8Pt3-8 indicates that Pt (3 wt%) was deposited on the carbon support (A8) and presents a particle size of 8 nm.

The morphology of support was studied by scanning electron microscopy (SEM) using a LEO (Carl Zeiss) GEMINI-1530 microscope. Textural characterization was carried out by N₂ and CO₂ adsorption at -196 °C and 0 °C, respectively, with a Quantachrome Autosorb-1 equipment. The BET and Dubinin-Radushkevich equations were applied to determine the apparent surface area (S_{BET}) and the micropore volume (W₀), the mean micropore width (L₀) and the microporous surface (S_{mic}), respectively [26–29]. The total pore volume was considered as the volume of N₂ adsorbed at P/P₀ = 0.95 [30].

Pt dispersion (D) and mean particle size (d) were obtained by H₂-chemisorption. The H₂-chemisorption isotherms were measured at 25 °C. The metal dispersion is obtained from the amount of H₂-chemisorbed assuming a stoichiometric ratio H₂:metal = 1:2 (dissociative chemisorption) and the average particle size was calculated as d_M(H₂) = k/D (nm) (k = 1.08 for Pt, 0.91 for Ru and 1.11 for Ir) [31–36]. HRTEM experiments were carried out using a Phillips CM-20 microscope equipped with EDAX microanalysis system and microphotograph analyzed by the appropriate software (ImageJ) in order to obtain the particle size distributions and the average particle size. Also powder X-ray diffraction (XRD) pattern were made using a Bruker D8 Advance X-ray diffractometer with Cu K α radiation at a wavelength (λ) of 1.541 Å. The 2θ angles were scanned from 20 to 70°.

The chemical characterization of the catalysts was further analyzed by X-ray photoelectron spectroscopy (XPS). The spectra were

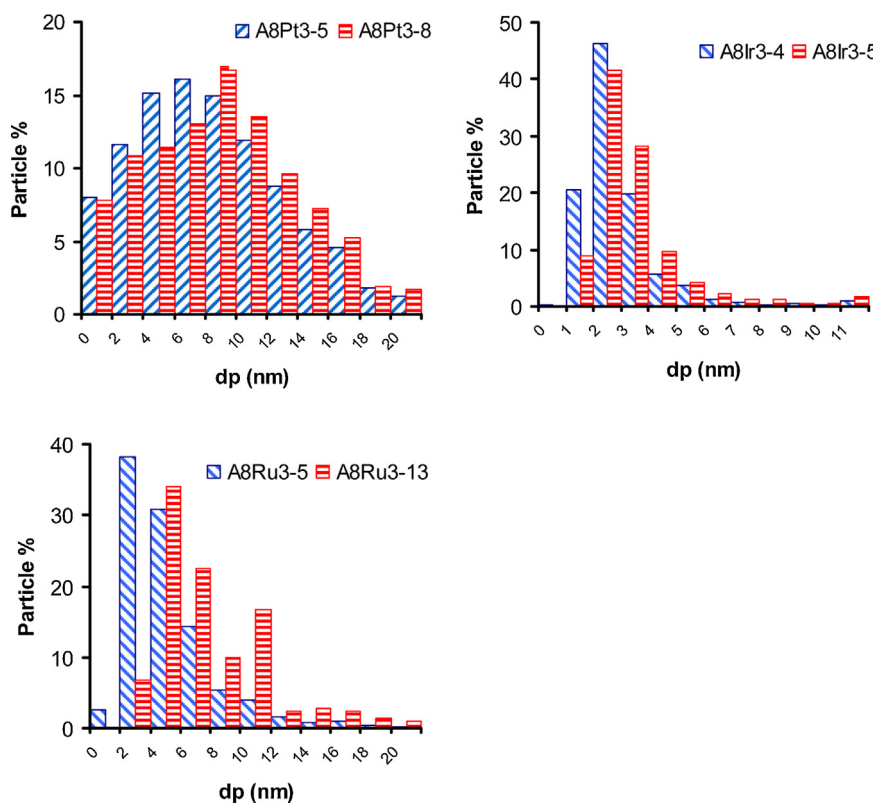


Fig. 4. Metal-particle size distribution obtained from HRTEM images.

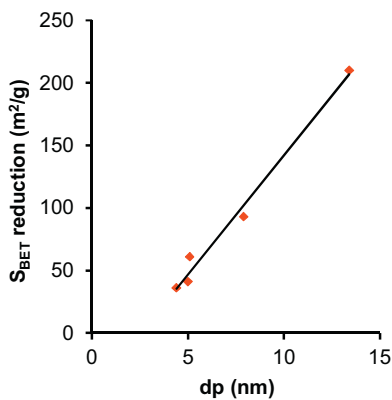


Fig. 5. Relationship between the surface area blockage of catalysts and the mean metal-particle size formed after each pretreatment.

obtained on a Kratos Axis Ultra-DLD X-ray photoelectron spectrometer equipped with a hemispherical electron analyzer connected to a detector DLD (delay-line detector).

Thermogravimetric (TG) experiments of used catalysts were carried out in N₂-flow with coupled-FTIR analysis of the evolved gases (TPD) in order to obtain information about the amount and nature of organic compound deposits. In this sense, desorbed gases (CO, CO₂, H₂O and aliphatic rest, CH₄) were simultaneously analyzed.

The citral hydrogenation was carried out in 100 ml heptane solution at a constant hydrogen pressure of 8.3 bar and 90 °C using a batch reactor model 5500 from Parr. The experimental conditions: citral concentration, catalyst weight and agitation speed were previously optimized in order to avoid mass transfer limitations (results not shown) and fixed in 0.05 M, 500 mg and 1500 rpm, respectively. The catalyst previously was pretreated outside the

reactor and then quickly transferred to the reactor. A small volume of sample was periodically withdrawn and analyzed by chromatography using a Bruker 430-GC equipped with a FID detector and a Varian GC (25 m × 0.32 mm × 0.45 µm) column. Citral and other products were previously calibrated.

After the reaction, the catalyst is recovered by filtering and washed several times with heptane before reuse without any additional treatment, but keeping constant the ratio catalyst/citral as well as the rest of experimental conditions.

3. Results and discussion

3.1. Morphology and textual characterization

The textural and morphological properties of different inorganic and carbon supports, including carbon xerogels, were optimized in previous works [14,15]. The best performance in the citral hydrogenation was obtained using microporous materials structured in microspheres [15], Fig. 2a. This material was selected now to develop a catalysts series based on different metals (M = Pt, Ru, Ir). The textural characteristics of support and their respective pre-treated M-catalysts are summarized in Table 1. It is well known that N₂ and CO₂ adsorption provides complementary information about microporosity [37]. Thus, the narrow microporosity, corresponding to micropores with diameter lower than 0.7 nm, is determined by CO₂, while the total microporosity is obtained from N₂ isotherm in absence of diffusion restrictions. Thus, the volume of N₂ adsorbed close to saturation ($P/P_0 = 0.95$; $V_{0.95}$) was considered as the total pore volume of the samples [30]. All the N₂-adsorption isotherms obtained correspond to type I, and the results obtained from them (Table 1), point out that A8-support is a microporous material, with a null mesopore volume (V_{meso}), but that exhibits an important macropore volume as detected by mercury porosimetry ($V_{macro} = 3.91 \text{ cm}^3 \text{ g}^{-1}$). Microporosity is intrinsic of the carbon

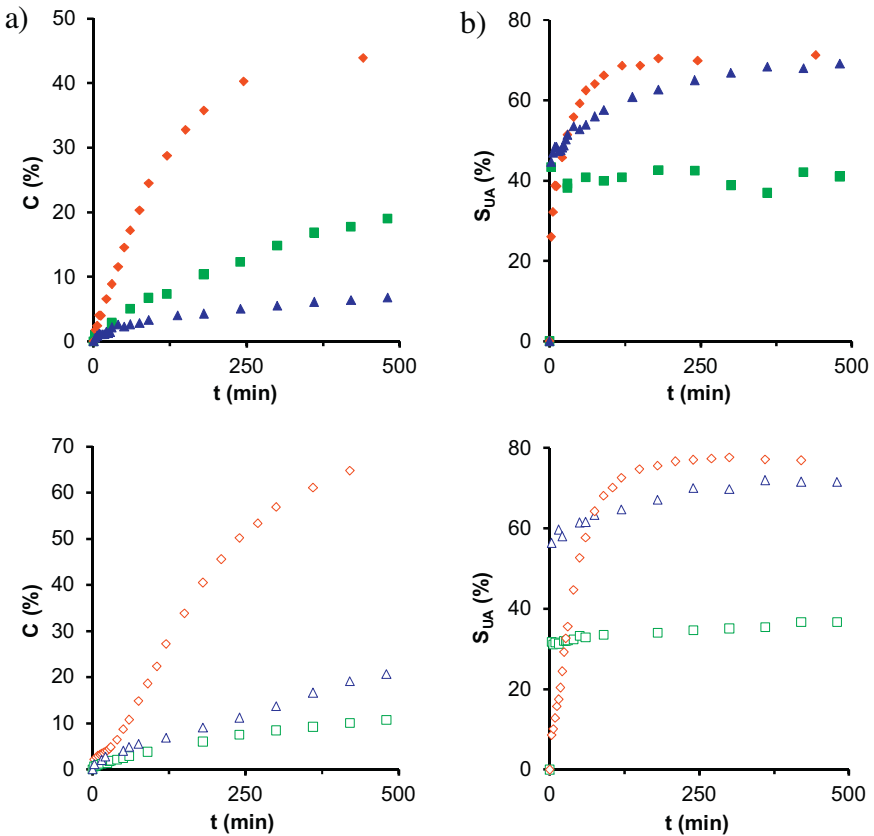


Fig. 6. Conversion (a) and S_{UA} (b) obtained with 3% metal-loading catalysts (\blacktriangle Ir, \blacklozenge Pt, \blacksquare Ru) supported on carbon xerogel after He-pretreatment (closed symbols) and H_2 -pretreatment: open symbols.

microspheres, being mainly formed during carbonization by the release of gases [38], while large interparticle voids (macropores) are generated between them. The pore size distribution (PSD) (Fig. 2b) obtained in this case, shown two maxima clearly located at the micrometer range. Catalysts present smaller micropore volumes and specific surface areas than their corresponding supports, denoting a certain micropore blockage after the deposition of metal-particles. The total pore volume detected by N_2 -adsorption ($V_{0.95}$) progressively decreases with increasing the metal-particle size detected. However macroporosity does not change, confirming the interparticle character of this porosity range.

3.2. Metal-characterization: nature and dispersion

It is well known that the hydrogenation of α - β unsaturated aldehydes is strongly dependent on metal dispersion [2,13,23]. In this catalyst series, the metal dispersion was tentatively modified by changing the pretreatment conditions. As commented in the experimental section, chemical state and dispersion of metals were analyzed by XPS, XRD, H_2 -chemisorption and TEM measurements. Results are summarized in Table 2, some representative TEM micrographs are shown in Fig. 3 and the metal-particle distribution calculated from them in Fig. 4. In general, the metal-particle size values obtained by TEM and H_2 -chemisorption (Table 2) present a similar evolution. TEM images show a very high density of metal-nanoparticles on the spherical particles of the carbon support being sintering favored after H_2 -pretreatment (Fig. 3). Some large particles are always observed by TEM together a majority of smaller ones. H_2 -chemisorption only provides a mean particle size, however, even this technique also clearly point out that H_2 -pretreatment favors the metal sintering regarding the He-one, being this effect stronger in the sense Ir < Pt < Ru. This is also showed

by the significant shifting of the particle size distribution measured for Ru-catalysts after each pretreatment (Fig. 4).

Similarly, XPS results show that in all cases the surface metal content ($M_{XPS}\%$) is larger than the theoretical loading (3%), indicating a higher metal concentration on the external surface. This parameter decreases after the H_2 -pretreatment regarding the He-one, as consequence of the greater metal-particle size obtained. Due to the absence of mesoporosity in the support, and because always the mean metal particle size exceeds the micropore size (2 nm) these particles should be formed preferentially on the outer surface of the carbon microspheres, as is also denoted by HRTEM images.

The different metal-particle size and distribution influence the final porous texture and specific surface area of the catalysts. Thus, it is noteworthy that the S_{BET} decreases linearly with increasing the metal particle size (Fig. 5). Metal particles are blocking or partially filling the larger micropores, as denoted by the reduction of both W_0 (N_2) and L_0 (N_2) values (Table 1), however, these parameters remain constant regarding A8 support for all the pretreated catalysts for the narrower microporosity (micropores smaller than 0.7 nm) determined by CO_2 adsorption. These results mean that the larger micropores (0.7–2 nm of diameter) are related with the high and homogeneous distribution of metal particles on the carbon microspheres surface observed by HRTEM, but not the narrowest ones.

Regarding the chemical state of the different metals XPS analysis pointed out a mixture of $M(0)/M(II)$ species in all the catalysts, the ratio is more or less independent on the metal and pretreatment used. In all cases there is a fraction of reduced metal around 70%, the oxidized phase can be formed during the storage in air before the analysis. However, XRD only shown peaks corresponding to the M^0 -species, indicating that the oxidized one can be

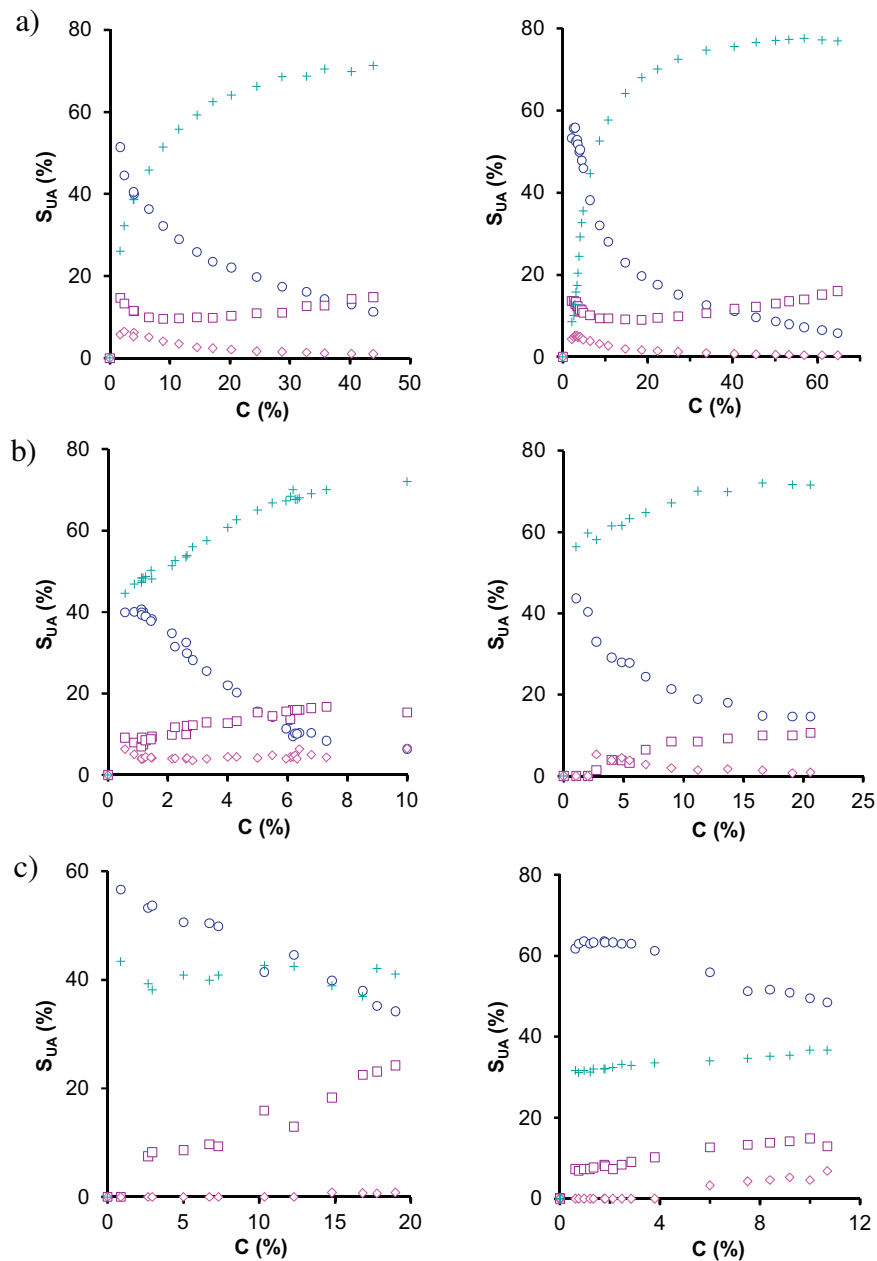


Fig. 7. Products selectivity as a function of the conversion reached (500 mg of catalyst, 1500 rpm, 0.05 M citral, $\text{PH}_2 = 8 \text{ bar}$, 90°C): citronellal (\circ) citronellol (\square), 3,7-dimethyloctanol (\diamond), S_{UA} (+). (a) A8Pt3, (b) A8Ir3, (c) A8Ru3. Left: He-pretreatments, right: H₂-pretreatments.

amorphous particles or be formed on the more reactive parts of the M^0 -nanoparticles (imperfections, borders, grain limits, etc) either by interaction with the air or with the oxygen content of the carbon surface.

3.3. Catalytic performance

Because all catalysts present a similar metal particle size after He-pretreatment ($4.7 \pm 0.4 \text{ nm}$, Table 2), the influence of metal dispersion is avoided and comparisons between active phases can be analyzed directly. The evolution of the conversion and selectivity values along the reaction is showed in Fig. 6 and a comparison of the initial reaction rates (r_0) and the products selectivity at low conversion values is presented in Table 3. Clearly, the catalytic activity increases in the sense $\text{Ir} < \text{Ru} < \text{Pt}$ (Fig. 6a). As commented, the low activity of Ir-catalysts is in agreement with previous studies [7].

Similar conclusions are obtained by comparing the initial reaction rate (Table 3).

Initially, the selectivity to the most valuable unsaturated alcohols varies as $\text{Ir} > \text{Ru} > \text{Pt}$, i.e. shows the contrary tendency that the catalytic activity (Fig. 6b and Table 3). However, while S_{UA} present constant values (at around 40%) in all the conversion range obtained when use Ru-catalyst, significantly increases along reaction for Ir and Pt-catalysts. This increase is slower in the case of the Ir-catalyst and stronger and faster for Pt-catalyst. Although S_{UA} reaches in both cases a similar value (around of 70%) after 8 h of reaction, it is noteworthy the different conversion values obtained at this reaction time.

After H₂-pretreatment sintering is favored in the sense $\text{Ir} < \text{Pt} < \text{Ru}$. The catalytic performance changes regarding He-pretreatment are directly related with the sintering degree. Thus, the slow increase in the metal particle size of Ir-catalysts mainly

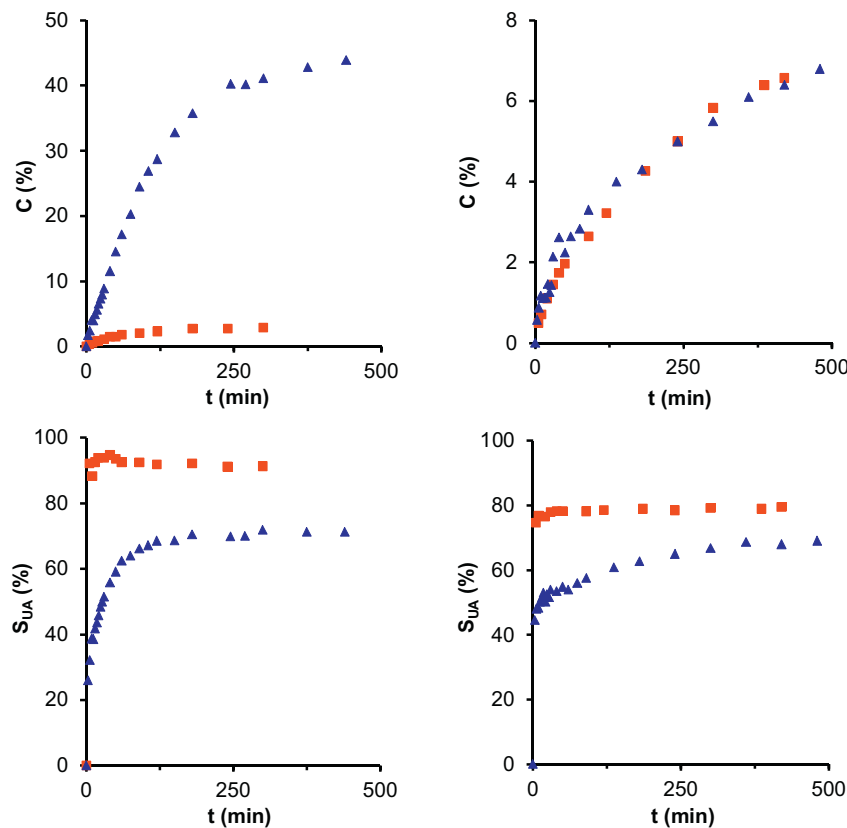


Fig. 8. Evolution of conversion and selectivity values in two consecutive reaction cycles. Left A8Pt3-5, right A8Ir3-4. (▲) First cycle, (■) second cycle.

favor the activity (final conversion at 480 min is practically twice than for He-pretreated catalyst) without influencing significantly selectivity values (final S_{UA} values around 70%), the moderate sintering of Pt favors both activity (that increase from 40 to 65%) and selectivity, however, in the case of the Ru-catalyst, where sintering is stronger (Table 2), conversion clearly decreases to the half with a simultaneous decrease of the S_{UA} values. These results pointed out that both activity and selectivity present an optimum for metal-particle size. Thus, probably the catalytic performance (mainly activity) of Ir-catalysts could be enhanced by increasing slowly the metal particle size, while the selectivity values for Ru-catalyst seem to be always around 40%. All this, confirms that the selective hydrogenation of citral is structure sensitive for all tested active phases. Galvagno et al. [39], using Ru/activated carbon as catalyst found that, in the case of citral, where no aromatic ring is present, the steric effect cannot play an important role, and therefore, no difference in the product distribution is observed with a change of the metal particle size ranging from 3 to 16.8 nm.

It is noteworthy that when Pt is supported on a carbon xerogel generates both the most active and the most selective catalyst. Ir-supported catalyst provides similar selectivity to unsaturated alcohol that Pt-catalyst but the yield to these products is smaller by its smaller activity. The yield of UA still decreases using Ru-catalysts (A8Ru3-5), which shows an intermediate activity and selectivity.

The significant differences in activity between Pt and Ir can be explained on the basis of the D-character, which is an empirical indicator of the electronic structure of the metal, and refers to the contribution of the D-electrons to the spd hybrid orbitals assumed in Pauling's resonance valence band theory [8] and electronic effects [2,22]. The correlation of the TOF with percentage of D-character was made by Singh and Vannice [8] obtaining a volcano plot where Pd and Pt have the higher activity and Ru and Ir have similar low activity in term of TOF. The electrostatic interactions of

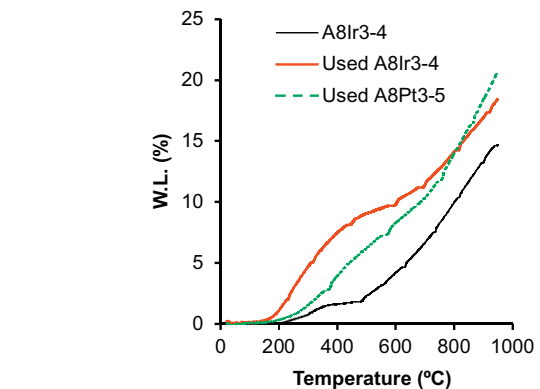


Fig. 9. Thermogravimetric analysis of fresh and used catalysts.

metal particles with the double bonds of the reactant molecules also determine their selectivity. Increasing electron density and hence D-orbital population, the repulsive four electron interaction of the metal with the C=C double bond increase while with the C=O π -system is favored [5,23].

When analysing the complete products distribution obtained in each case (Fig. 7) it is observed that UA are formed preferentially at the reaction beginning only in the case of Ir-catalysts, while citronellal is main product obtained using either Pt or Ru-catalysts. The S_{UA} remains constant along reaction when use Ru-catalysts, independently the pretreatment used. In this case, with increasing conversion secondary hydrogenation processes from citronellal to citronellol are favoured, but the complete hydrogenation to 3,7-dimethyloctanol is not observed. In the case of Pt-catalysts, the strong increase of S_{UA} is accompanied by a simultaneous decrease of selectivity values to citronellal. Similarly, the formation of

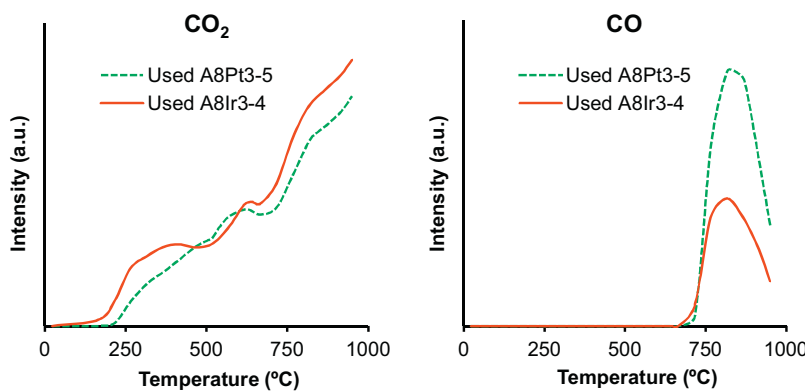


Fig. 10. TPD-profiles of CO_2 and CO evolved from Ir and Pt-catalysts after a first cycle of citral hydrogenation.

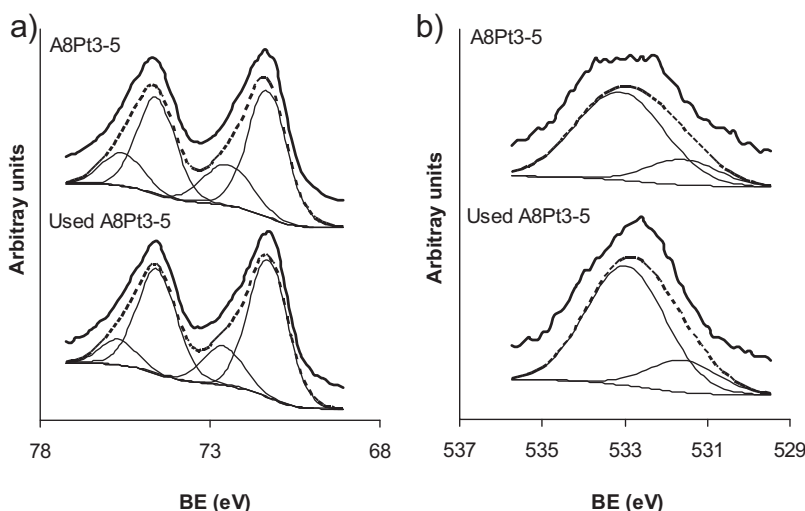


Fig. 11. (a) Platinum (Pt $4f$) and (b) oxygen (O $1s$) XPS spectral regions of fresh and used A8Pt3-5 catalyst.

citronellol and 3,7-dimethyloctanol also decreases, this fact indicates that these compounds are formed preferentially by a consecutive hydrogenation of citronellal regarding UA hydrogenation. Nevertheless the selectivity to citronellol slowly increases at high conversion values, when mainly UA are present, indicating that this process cannot be completely neglected. A similar but slower formation of other products can be described for Ir-catalysts. UA are formed instead citronellal, increasing slowly the citronellol at high conversion values by hydrogenation of UA. Also, note that cracking reactions as well as cyclization reactions are not observed. Both reactions are related with the catalysts acidity, which in turn, is also influenced by the presence of Cl^- ions from the metal precursors [40]. Thus, the influence of these parameters can be neglected in this catalyst series.

These results point out that at the reaction beginning there are some transformations in Pt and Ir-catalysts that deactivate the more active phase is analyzed to find centres where the C=C hydrogenation occurs, favouring the hydrogenation of the C=O bonds and the formation of UA. In such a basis, used Ir and Pt-catalysts could be consequently more selective to UA than their corresponding fresh samples and therefore, the reuse of these samples seems to be quite interesting. Ru-catalysts are not included in this study due to the lower performance detected. The results obtained after a second hydrogenation cycle are compared in Fig. 8.

It is observed that the performance of Ir-catalysts is improved; although the commented low activity of this catalyst, conversion values are maintained regarding the first hydrogenation cycle but,

as expected, the selectivity increases showing very high S_{UA} values ($S_{\text{UA}} > 80\%$). However, in the case of Pt-samples, catalyst is clearly deactivated, conversion values become very low (but still in the range obtained with Ir-catalysts) and UA is practically the unique product.

To elucidate this behavior, the used catalysts were analyzed from a textural and chemical point of view. These changes should be associated to modification in the chemical and porous characteristics of supports, because no metal-leaching or sintering was observed by analysing both the liquid reaction media and the recovered solid catalysts.

The first question is to determine the amount of possible deposits formed on the catalyst surface. Because the mass balances indicate a good agreement between the amount of reactants and reaction products, the amount of these deposits should be low. Nevertheless, a deep pore blockage of the support porosity was observed; the BET surface area decrease from $580 \text{ m}^2 \text{ g}^{-1}$ to around $10 \text{ m}^2 \text{ g}^{-1}$ in both cases. Because metal particles, as discussed, are located on the external surface, the microporosity blockage should not influence the accessibility of reactants to the metallic centers, and consequently deactivation, as clearly observed for Ir-catalysts (Fig. 8). Thus, deactivation should be related to chemical transformation of the catalysts surfaces.

Due to the carbon support nature, it is impossible to determine the exact content of these organic deposits by burning. Nevertheless, TG-experiments carried out in N_2 -flow with coupled-FTIR analysis of the evolved gases (TPD) can provide some information

about the amount and nature of such deposits. In this case, desorbed gases (CO , CO_2 , H_2O and aliphatic rest, CH_4) were simultaneously analyzed. In Fig. 9 the weight loss (WL) detected for Pt and Ir-catalysts after the first reaction cycle are shown. Fresh Ir-catalyst is used as blank sample. It is observed that in both used samples the WL increases regarding the fresh one. The used Ir-catalyst shows higher WL than the Pt-ones bellow 600°C , while from this temperature range this parameter quickly increase in the last case. These results indicate that both metals induce the formation of deposits with different chemical nature.

These differences are also noticed by analyzing the nature of the gases evolved during the TG experiments. The formation of CO and CO_2 by decomposition of oxygenated groups located on the carbon surface is well documented [41,42]. Thus, CO_2 can be evolved from carboxylic acid groups that decompose at low temperature (typically bellow 400°C) while lactones can be stable up to 700°C . Other oxygenated structures like phenols, ether or quinones are evolved as CO and they are in general thermally more stable than those evolved as CO_2 , typically evolving from 600°C . In our case, because supports are obtained at high temperature and catalysts were previously reduced the oxygen content was estimated below 0.8% wt.; oxygenated surface groups should be generated mainly along citral reactions, being mainly associated to adsorbed rest of citral or their derivatives products. As commented, the deposit generated on Ir-catalysts present a smaller thermal stability than those formed on Pt-catalyst, as demonstrated by TG. This fact is also accompanied by a larger amount of CO_2 evolved (Fig. 10). CO-desorption was only observed at high temperature, i.e. is due to the decomposition of more stable oxygenated species. In this case, the amount of CO-evolved is higher in the case of used Pt-catalysts.

The enrichment of the support surface with oxygenated deposits change the nature of this surface from hydrophobic to hydrophilic, which favors the citral adsorption through $\text{C}=\text{O}$ bond and consequently the UA formation [14]. This fact is observed for both Ir-and Pt-catalysts (Figs. 7,8), while the Ru-one seems to be unaffected by this change. Nevertheless, the importance of the nature of these deposits plays an important role on the stability of the catalyst. Thus, while the activity of Ir-catalyst is maintained, the deactivation of Pt-hydrogenation centers by formation of adsorbed deposits was observed. This fact was also previously described by different authors [43,44], showing that irreversibly chemisorbed CO , formed by decomposition of citral molecules, can deactivate the active Pt-sites.

Taking into account the strong deactivation of Pt-catalysts, the used catalysts were also studied by XPS. Results point out an increase of the surface oxygen content from 3.0 to 4.6%, whereas the Pt content detected do not change significantly regarding the fresh sample (from 7.0 to 7.3%) being also constant the Pt/Pt^{+2} ratio (72.5%); the corresponding spectral regions are showed in Fig. 11. These results also confirm that leaching or sintering do not occurs during reaction and that adsorbed organic rest are located mainly on the carbon surface, blocking micropores.

4. Conclusions

A series of supported catalysts is obtained by impregnation of a carbon xerogel structured in microspheres with different active phases (Pt, Ru, Ir). Pretreatment in He -flow leads to a similar metal-dispersion, but sintering increases after H_2 -pretreatment mainly in the case of Ru-catalysts. In all cases, metal particles are formed exclusively on the external surface of microspheres because the microporous character of the support.

The catalytic activity varies in the sense $\text{Pt} > \text{Ru} > \text{Ir}$, while the most selective catalysts are obtained with Pt and Ir. Thus the higher UA yield is obtained using Pt-catalysts. The catalytic performance

is favored by increasing the metal-particle size up to 8–10 nm. The large sintering detected for Ru-catalysts provoke a diminution of both activity and selectivity. An intrinsic selectivity of around 40% is detected for Ru-catalysts along the reaction, while this parameter clearly increases during reaction either for Pt and Ir-catalysts, suggesting an interesting reuse of samples.

The reutilization experiments point out that this is possible for Ir-catalysts but a strong deactivation is found in the case of Pt-catalysts. This is related with the formation of highly stable CO-species poisoning the Pt-active sites.

Acknowledgements

This research has been supported by the Spanish projects P12-RNM-2892 and CTQ2013-44789-R, from Andalucia's government and MINECO, respectively. EBG acknowledges for a pre-doctoral fellowship to the MCINN project CTM2010-18889.

References

- [1] T. Ekou, A. Vicente, G. Lafaye, C. Espel, P. Marecot, *Appl. Catal. A: Gen.* 314 (2006) 64–72.
- [2] F. Delbecq, P. Sautet, *J. Catal.* 152 (1995) 217–236.
- [3] T. Ekou, L. Ekou, A. Vicente, G. Lafaye, S. Pronier, C. Espel, P. Marecot, *J. Mol. Catal. A: Chem.* 337 (2011) 82–88.
- [4] H. Surburg, J. Panten, *Common Fragrance and Flavor Materials: Preparation, Properties and Uses*, WILEY-VCH, Weinheim, Germany, 2006.
- [5] P.Y. Claus, Önal, regioselective hydrogenations, in: G. Ertl, H. Knözinger, F. Schüth, J. Weitkamp (Eds.), *Handbook of Heterogeneous Catalysis*, WILEY-VCH, Weinheim (Germany), 2008, pp. 3311–3312.
- [6] A. Vannice, U.K. Singh, *Abstr. Pap. Am. Chem. Soc.* 223 (2002) 437.
- [7] E. Bailón-García, F.J. Maldonado-Hódar, A.F. Pérez-Cadenas, F. Carrasco-Marín, *Catalysts* 3 (2013) 853–877.
- [8] U.K. Singh, M.A. Vannice, *J. Catal.* 199 (2001) 73–84.
- [9] P. Mäki-Arvela, J. Hájek, T. Salmi, D. Yu Murzin, *Appl. Catal. A: Gen.* 292 (2005) 1–49.
- [10] B. Coq, P.S. Kumbhar, C. Moreau, P. Moreau, M.G. Warawdekar, *J. Mol. Catal.* 85 (1993) 215–228.
- [11] V. Ponec, *Appl. Catal. A: Gen.* 149 (1997) 27–48.
- [12] S. Galvagno, C. Milone, A. Donato, G. Neri, R. Pietropaolo, *Catal. Lett.* 17 (1993) 55–61.
- [13] A. Giroir-Fendler, D. Richard, P. Gallezot, *Catal. Lett.* 5 (1990) 175–181.
- [14] E. Bailón-García, F. Carrasco-Marín, A.F. Pérez-Cadenas, F.J. Maldonado-Hódar, *Appl. Catal. A: Gen.* 482 (2014) 318–326.
- [15] E. Bailón-García, F. Carrasco-Marín, A.F. Pérez-Cadenas, F.J. Maldonado-Hódar, *Catal. Commun.* 58 (2014) 64–69.
- [16] D. Sokolskii, N. Anisimova, A. Zharmagambetova, S. Mukhamedzhanova, L. Edygenova, *React. Kinet. Catal. Lett.* 33 (1987) 399–403.
- [17] A. Giroir-Fendler, D. Richard, P. Gallezot, Heterogeneous catalysis and fine chemicals, in: M. Guisnet, J. Barrault, C. Bouchoule, D. Duprez, C. Montassier, G. Perot (Eds.), *Studies in Surface Science and Catalysis*, vol. 41, Elsevier Amsterdam, 1988, p. 171.
- [18] P. Reyes, H. Rojas, G. Peccati, J.L.G. Fierro, *J. Mol. Catal. A: Chem.* 179 (2002) 293–299.
- [19] H. Rojas, G. Borda, P. Reyes, J.J. Martínez, J. Valencia, J.L.G. Fierro, *Catal. Today* 133 (2008) 699–705.
- [20] P. Chen, J.Q. Lu, G.Q. Xie, G.S. Hu, L. Zhu, L.F. Luo, W.X. Huang, M.F. Luo, *Appl. Catal. A: Gen.* 433–434 (2012) 236–242.
- [21] G. Borda, H. Rojas, J. Murcia, J.L.G. Fierro, P. Reyes, M. Oportus, *React. Kinet. Catal. Lett.* 92 (2007) 369–376.
- [22] F. Delbecq, P. Sautet, *J. Catal.* 211 (2002) 398–406.
- [23] P. Claus, *Top. Catal.* 5 (1998) 51–62.
- [24] S. Morales-Torres, F.J. Maldonado-Hódar, A.F. Pérez-Cadenas, F. Carrasco-Marín, *Phys. Chem. Chem. Phys.* 12 (2010) 10365–10372.
- [25] E. Gallegos-Suárez, A.F. Pérez-Cadenas, F.J. Maldonado-Hódar, F. Carrasco-Marín, *Chem. Eng. J.* 181–182 (2012) 851–855.
- [26] S. Brunauer, P.H. Emmett, E. Teller, *J. Am. Chem. Soc.* 60 (1938) 309–319.
- [27] M.M. Dubinin, *Carbon* 23 (1985) 373–380.
- [28] M.M. Dubinin, *Russ. J. Phys. Chem.* 39 (1965) 1305–1317.
- [29] F. Stoeckli, in: J. Patrick (Ed.), *Porosity in Carbons—Characterization and Applications*, Arnold, London, 1995.
- [30] R. Ubago-Pérez, F. Carrasco-Marín, D. Fairén-Jiménez, C. Moreno-Castilla, *Microporous Mesoporous Mater.* 92 (2006) 64–70.
- [31] J.E. Benson, M. Boudart, *J. Catal.* 4 (1965) 704–710.
- [32] G.R. Wilson, W.K. Hall, *J. Catal.* 17 (1970) 190–206.
- [33] C. Moreno-Castilla, M.A. Salas-Peregrín, F.J. López-Garzón, *J. Mol. Catal. A: Chem.* 95 (1995) 223–233.
- [34] F. Rodríguez-Reinoso, J. de Dios López-González, C. Moreno-Castilla, A. Guerrero-Ruiz, I. Rodríguez-Ramos, *Fuel* 63 (1984) 1089–1094.
- [35] H. Kubicka, *J. Catal.* 12 (1968) 223–237.

- [36] P. Reyes, M.C. Aguirre, G. Pecchi, J.L.G. Fierro, *J. Mol. Catal. A: Chem.* 164 (2000) 245–251.
- [37] D. Cazorla-Amorós, J. Alcañiz-Monge, A. Linares-Solano, *Langmuir* 12 (1996) 2820–2824.
- [38] C. Moreno-Castilla, F.J. Maldonado-Hódar, *Carbon* 43 (2005) 455–465.
- [39] S. Galvagno, C. Milone, A. Donato, G. Neri, R. Pietropaolo, *Catal. Lett.* 18 (1993) 349–355.
- [40] G. Neri, L. Mercadante, A. Donato, A.M. Visco, S. Galvagno, *Catal. Lett.* 29 (1994) 379–386.
- [41] C. Moreno-Castilla, F. Carrasco-Marín, F.J. Maldonado-Hódar, J. Rivera-Utrilla, *Carbon* 36 (1998) 145–151.
- [42] J.L. Figueiredo, M.F.R. Pereira, M.M.A. Freitas, J.J.M. Órfão, *Carbon* 37 (1999) 1379–1389.
- [43] D. Manikandan, D. Divakar, T. Sivakumar, *Catal. Lett.* 123 (2008) 107–114.
- [44] U.K. Singh, M. Albert Vannice, *J. Catal.* 191 (2000) 165–180.